

3D Printing of β -TCP/S53P4 Scaffolds: Physicochemical, Mechanical, and Biological *in vitro* Evaluation

Ana P.N. Alves¹, Lucas Barbosa¹, Rodrigo L.M.S. Oliveira¹, Julia Andrade de Oliveira², Mariana de Sá Alves², Luana Marotta Reis de Vasconcellos² and Eliandra de S. Trichês^{1,*}

¹*Bioceramics Laboratory, Instituto de Ciência e Tecnologia, Universidade Federal de São Paulo – UNIFESP, 12231-280, São José dos Campos, SP, Brazil*

²*Department of Bioscience and Oral Diagnosis, Institute of Science and Technology of São José dos Campos, São Paulo State University - UNESP, 12245-000, São José dos Campos, São Paulo, Brazil*

Abstract: The focus of bone tissue engineering is on the new strategies for developing bioactive and resorbable scaffolds, which have become an alternative to the treatment of bone diseases and trauma. β -tricalcium phosphate (β -TCP) is considered resorbable and has excellent osteoconductivity. In an attempt to achieve good densification of the β -TCP scaffold and improve its biological properties, it arises the possibility of combining this material with S53P4 bioactive glass. Several techniques are used to produce bioceramic scaffolds, among them, direct ink writing (DIW) a type of additive manufacturing based on material extrusion, which allows the production of customized parts, with high complexity and good reproducibility. This work prepared β -TCP and β -TCP/S53P4 (β -TCP/10-S53P4 = 10% wt of S53P4 and β -TCP/20-S53P4 = 20% wt of S53P4) scaffolds by DIW. The ceramic inks showed pseudoplastic behavior and the 3D-printed scaffolds showed similar aspects to the digital model. Also, the β -TCP/S53P4 scaffolds (β -TCP/10-S53P4 = 1.6 ± 0.6 MPa and β -TCP/20-S53P4 = 2.1 ± 0.9 MPa) showed an increase in compressive strength when compared to β -TCP scaffolds (0.9 ± 0.1 MPa). All scaffolds showed apatite-mineralization ability in SBF after soaking for 7 and 14 days, being that the β -TCP/20-S53P4 scaffold showed a higher ability of apatite formation compared to the other scaffolds. Concerning the biological *in vitro* assays, all the scaffolds showed good cell viability. Thus, the β -TCP/S53P4 scaffolds showed adequate properties which become them, good candidates, to be used in bone tissue engineering.

Keywords: β -tricalcium phosphate, Bioactive glass S53P4, Scaffolds, 3D printing.

1. INTRODUCTION

For years, research on bone tissue engineering has been trying to develop an artificial bone graft capable of surpassing autologous grafts. Autologous grafts are limited by the low quantity available to transplant and by complications that may arise during the harvesting procedure [1-5]. Regardless, to this day, they still are the gold standard material to promote bone regeneration. Among the artificial bone grafts, bioceramic scaffolds have been showing promising results. They combine the scaffold's porous structure with the regenerative potential of bioceramics, resulting in a material similar to the cancellous bone matrix [6-9]. However, they are limited by their brittleness, which impairs their application to the defect with complex geometry, and by their low mechanical resistance [7-9].

Additive manufacturing techniques (AM) allow for overcoming the geometrical limitations of ceramic scaffolds [10]. Due to their great control over the scaffolds' final structure, AM enables the production of customizable scaffolds with a perfect fit to the defect geometry [11-15]. Among the AMs, direct ink writing

(DIW) is one of the most employed methods in the production of ceramic scaffolds [16-18]. This is a 3D-printing technique based on material extrusion. The scaffolds are produced by printing a colloidal ink, which is stored in a reservoir and extruded through a nozzle to form a filament. A layered pattern is drawn by moving the nozzle to achieve the printing of the scaffold. The final scaffold is formed by stacking the printed layers and its geometry is foreseen in CAD software, including its shape, total porosity, and pores morphology. Some parameters are essential for the success of the process such as the ink rheological properties [16]. A good relation among viscosity, shear stress, and shear rate are necessary to facilitate ink extrusion and shape retention [16].

Among the ceramics applied to bone regeneration, calcium phosphates stand out due to their chemical similarity to the mineral bone matrix [19, 20]. They are capable of aiding in cell differentiation due to their dissolution *in situ* and of absorbing osteoinductive factors on their surface, creating a favorable environment for bone regeneration [21, 22]. Bone mineral matrix is highly similar to hydroxyapatite, containing some ionic substitutions in its structure [23-25]. However, the use of hydroxyapatite as a base material in scaffold manufacturing is limited by its slow

*Address correspondence to this author at the 330 Talim Street – Vila Nair, São José dos Campos, SP – Brazil, Zip Code: 12231-280; Tel: +55 12 3385 4253; E-mail: elianandra.sousa@unifesp.br

dissolution rate and low mechanical properties [26-28]. Thus, several other calcium phosphates are explored in scaffold manufacturing.

In contrast to the lack of solubility of hydroxyapatite, β -tricalcium phosphate (β -TCP) is a calcium phosphate that takes part in the bone metabolic cycle, being resorbed by osteoclasts while being replaced by new bone tissue [29, 30]. In addition, β -TCP has shown osteoinductive and osteoconductive properties, great cell adhesion, and the capability to aid in bone mineralization [22, 26, 31]. Those properties make β -TCP promissory as scaffolding material in bone tissue engineering. However, reaching high densification of β -TCP scaffolds during the sintering process is challenging once temperatures over 1120 °C can induce the transformation of α -TCP. As α -TCP has a lower density than β -TCP (2.86 and 3.07 g/cm³, respectively), its formation induces microcracks in the scaffold's structure and jeopardizes its mechanical resistance [32, 33].

In previous reports of our research group [34], it was shown that the mechanical resistance of β -TCP scaffolds can be improved by adding 5.0 and 7.5 wt.% of 45S5 bioactive glass (BG 45S5). The bioactive glass melts while sintering the scaffolds, filling microporosity and microcracks, thus, leading to a significant increase in their densification and mechanical resistance. Ma *et al.* [35] reported that the addition of BG 45S5 in 3D-printed β -TCP scaffolds also improves the degradation rate and proliferation of MC3T3-E1 pre-osteoblast cells. Recently, Hua *et al.* [36] reported that the addition of 45S5 in β -TCP scaffolds also enhances the mineralization in SBF.

BG 45S5 was developed by Larry Hench in 1969 [37, 38]. This material has a great biological response when implanted in bone defects, aiding in osteoblast proliferation, tissue mineralization, and stimulating angiogenesis [39, 40]. After the development of BG 45S5, several other compositions of bioactive glasses were developed throughout the years. Among them, S53P4 bioactive glass (BG S53P4) has been showing a great clinical outcome. BG S53P4 has been commercialized by Bonalive[®] since 2010 and has been applied successfully in the treatment of benign bone tumors, bone infections, spine corrections, and trauma reconstruction [41-43]. Despite its great clinical outcome, BG S53P4 is still hardly explored as a material for scaffold manufacturing when compared with other BGs compositions.

In this context, we report the production of 3D-printed β -TCP/S53P4 scaffolds, evaluating the effect of BG S53P4 content on the properties of the scaffold. A recent study from our group has shown great results regarding the association between β -TCP and S53P4 (7.5 wt.%) [44]. β -TCP scaffolds containing 0, 10, and 20 wt.% of BG S53P4 were produced by the DIW technique and evaluated regarding their physical and chemical properties, including the rheological behavior of the ink employed in their production. We also investigated the apatite-mineralization ability of the scaffolds in simulated body fluid (SBF) after soaking for 7 and 14 days, and the response of mesenchymal cells (MSC) towards the scaffolds, including cell adhesion and viability, total protein, and alkaline phosphatase (ALP) activity during MSC differentiation and nodules mineralization.

2. MATERIALS AND METHODS

2.1. Synthesis and Characterization of β -TCP Powder

The β -TCP powder was obtained by the solid-state reaction from a mixture of calcium carbonate (CaCO₃ – Synth) and calcium phosphate (CaHPO₄ – Synth), in a molar ratio of 1:2. The powder was calcined at 1050 °C for 6 hours in a muffle oven (EDG Equipamentos, EDG 10P-S). After that, the powder was milled in a ball mill (Marconi, MA-500) for 12 hours in aqueous suspension, using 84.5 wt.% of alumina balls (\varnothing = 6 mm), 10.9 wt.% of deionized water, and 4.6 wt.% of β -TCP powder in a 2 L polypropylene bottle.

The β -TCP powder was analyzed by X-ray diffraction (XRD, Rigaku, Ultima IV, 2θ from 20° to 60°, 0.02 ° s⁻¹), and the particle size distribution was determined by Laser Diffraction (Cilas, 1190L). The β -TCP presented a mean diameter of 1.13 μ m (d_{10} = 0.62 μ m, d_{50} = 1.06 μ m and d_{90} = 1.78 μ m).

2.2. Synthesis and Characterization of BG S53P4 Powder

BG S53P4 powder was obtained by the melting-quenching technique. Initially, the precursor oxides (53% SiO₂, 20% CaO, 23% Na₂O, and 4% PO₄, wt.%) were mixed in a horizontal ball mill (Marconi, MA 500) for 2 hours. The mixture was placed in a platinum crucible (Platimex, Brasil) and melted in a melting furnace (Fortlab, MEV 1700/V) at 1360 °C for 30 minutes. Then, the molten glass was poured into deionized water at room temperature for the quenching

process. The coarse BG S53P4 particles were dried at 70 °C overnight.

The milling process to obtain fine BG S53P4 particles occurred in three steps, as described in [45]. In the first step, the coarse particles of BG S53P4 were dry milled for 72 hours in a horizontal ball mill (Marconi, MA-500) using 80.8 wt.% of zirconia balls ($\varnothing = 5$ mm) and 19.2 wt.% of glass particles in a 1 L polypropylene bottle. The resulting glass powder was sieved through a 60 ASTM sieve (opening of 250 μm) and taken to the second milling step, a dry milled process in a high-energy mill (Servitech CT-241) for 10 minutes, using 75 wt.% of porcelain balls ($\varnothing = 12$ mm) and 25 wt.% of glass particles. The glass powder was sieved using a 140 ASTM sieve (opening of 106 μm), and, finally, wet-milled for 36 hours in a horizontal ball mill (Marconi, MA-500), using 87.0 wt.% of zirconia balls ($\varnothing = 2.5$ mm), 7.5 wt.% of isopropyl alcohol, and 5.5 wt.% of glass powder in a 500 mL polypropylene bottle. The final resulting glass powder was sieved using a 200 ASTM sieve (opening of 75 μm) and dried at 70 °C overnight.

The BG S53P4 powder was analyzed by X-ray diffraction (XRD, Rigaku, Ultima IV, 2θ from 20° to 60°, 0.02 ° s⁻¹), and the particle size distribution was determined by Laser Diffraction (Cilas, 1190L). The BG S53P4 presented a mean diameter of 3.85 μm ($d_{10} = 1.32$ μm , $d_{50} = 3.50$ μm and $d_{90} = 11.63$ μm).

2.3. Preparation of β -TCP and β -TCP/S53P4 Inks and Rheological Analysis

The ceramic inks were prepared using an alginate mixer (Biotron®, Fast). Over 8 minutes, the powders were slowly added to a 20 wt.% Pluronic solution (Pluronic® F127, Sigma-Aldrich) in the mixing bowl while the ink was homogenized. After adding all the powders, 2.65 wt.% (concerning total ink) of PEG (polyethylene glycol 400, Synth) was added to the ink, which was homogenized for more than 5 minutes. In this work, three compositions were studied, with variations in the amount of BG S53P4. They were 100 wt.% of β -TCP; 90 wt.% of β -TCP/10 wt.% of BG S53P4; and 80 wt.% of β -TCP/20 wt.% of BG S53P4, denoted as β -TCP, β -TCP/10-S53P4 and β -TCP/20-S53P4 scaffolds, respectively. All the inks were prepared with 53 wt.% of solids content and 47 wt.% of Pluronic solution.

The rheological behavior of the inks was analyzed using a torque rotational rheometer (Haake,

Rheostress 6000) based on Peng *et al.* [16] and Feilden *et al.* [46]. The analyses were carried out at 25 °C using parallel plate geometry (diameter of 35 mm and 1 mm gap). In dynamic analysis, the shear stress and viscosity were determined as a function of shear rate, between 10⁻² and 10² s⁻¹. In the oscillatory analysis, the behavior of the storage modulus (G') and loss modulus (G'') was evaluated as a function of shear stress, between 0 and 1000 Pa.

2.4. 3D Printing and Characterization of the β -TCP and β -TCP/S53P4 Scaffolds

The β -TCP and β -TCP/S53P4 scaffolds were prepared using a 3D printer (DuraPrinter3D, E01) adapted with a Nordson storage system of 30 cm³ (syringe barrel and adapter Optimum®, cod. 7012136 and 7012338, Nordson) and a nozzle with an opening of 580 μm (SmoothFlow Tapered Tips, cod. 7005009, Nordson).

The scaffolds were printed with a speed of 18 mm/s, adjusting the pressure between 2 and 4 bars (Tekna Air, CP 8.5/25 – 2P) to maintain a constant flow during the printing process. The scaffolds' geometry was programmed in the Slic3r software with a cylindrical geometry with 12 mm of diameter, 4.7 mm of height, a porosity of 65%, and rectilinear pore geometry. After the printing, the scaffolds were dried at room temperature for 24 hours and then subjected to a heat treatment at 750 °C for 60 minutes, with a heating rate of 1 °C/min, to eliminate the organic additives, following up the temperature of 1150 °C, with a heating rate of 2 °C/min, and remaining at this temperature for 120 minutes, to sintering (Furnace - Jung, LF00914). The cooling process followed to room temperature, at the furnace's default cooling rate.

Scanning electron microscopy (SEM - FEI, Quanta) was used to evaluate the structure and morphology of β -TCP and β -TCP/S53P4 scaffolds. Energy-dispersive X-ray spectroscopy (EDS - FEI, Quanta) was performed for surface characterization and elemental quantification. Additionally, elemental mapping was performed at random spots on the scaffold surface. The test was run at 15 kV and a working distance of 10 mm. Scaffolds were previously covered with gold (Quorum, Q150R ES). X-ray diffraction (XRD – Rigaku, Ultima IV with CuK α detector and Ni filter, 2θ from 20° to 60°, 0.02 ° s⁻¹) was used to determine the crystalline phase of the β -TCP and β -TCP/BG S53P4 scaffolds. The compressive strength of β -TCP and β -TCP/S53P4 scaffolds was evaluated using a universal testing

machine (Emic, DL20000) with a load cell of 5 kN, speed of 0.5 mm/min, four scaffolds were used for each composition. The dimensions of the scaffolds were 12 mm in diameter and 20 mm high.

2.5. Apatite Mineralization Ability of the β -TCP and β -TCP/S53P4 Scaffolds

The apatite mineralization ability of the β -TCP and β -TCP/S53P4 scaffolds was investigated *in vitro* (n=3). The simulated body fluid (SBF) was prepared following the methodology described by Kokubo *et al* 1990 [47] and Kokubo *et al* 2006 [48]. The scaffolds were soaked in SBF solution for 7 and 14 days at 37 °C. The SBF solution was refreshed after soaking every 3 days. After collection, the scaffolds were dried at 100 °C overnight. The apatite formation on the scaffolds' surface was observed by X-ray diffraction (XRD, Rigaku, Ultima IV, 2 θ from 10° to 60°, 0.02 ° s⁻¹) and scanning electron microscopy (SEM - FEI, Quanta).

2.6. In vitro Biological Assays

2.6.1. Isolation MSC

The mesenchymal cells (MSC) were obtained from the femurs of nine Wistar rats (*Rattus norvegicus*). After cleaning the femurs, in the laminar flow, the bone marrow cells were isolated and inserted in cell culture flasks of 250 mL and 75 cm² (TPP, Biosystems, Curitiba, Brazil) with essential alpha MEM medium culture (Gibco) supplemented with 10% Bovine Fetal Serum (SBF) (LGC Technology, Campinas, Brazil) and gentamicin (500 μ g / mL) (Gibco) and were incubated at 37 °C, with atmospheric humidity containing 5% carbon dioxide (CO₂). The culture medium was changed every three days and the progression of the culture was evaluated by inverted phase microscopy (Microscope Carl Zeiss – Axiovert 40C, Germany). After confluence (approximately seven days), cells were released enzymatically and plated at a density of 2 x 10⁴ viable cells in each well of the 24-well microplate (TPP, Biosystems, Curitiba, Brazil) as previously described [49]. Previously to the plating, the samples were sterilized in UV light and then placed inside the wells. The control group was represented only by cells in the wells. Following this, the osteogenic culture medium was added to the plate, which was changed every 48 hours.

After these procedures, all plates were incubated at 37 °C with 5% CO₂ and kept until the time of the tests described below. All tests were performed according to

ISO 10993-5 [50] and in triplicate, with each isolation being a pool of cells from the femur of three animals.

2.6.2. Cell Morphology

After 5 days of cultivation, cell morphology was evaluated by SEM (FEI, Quanta). The samples with cells were fixed with 4% paraformaldehyde and were dehydrated with ethanol, then the samples were coated with gold using a sputter-coating system (Quorum, Q150R ES, parameters 20 mA, and 90 s).

2.6.3. Cell Viability

After 7 days, a quantitative assessment of live cells was performed, after exposure to a solution of MTT (3-(4,5-dimethylthiazole bromide – Sigma-Aldrich), and the formazan crystals were dissolved by adding dimethyl sulfoxide solvent (DMSO – Sigma-Aldrich) into each well. The plates were shaken at room temperature, and after the dissolution of the crystals, the absorbance was measured spectrophotometrically at 570 nm (Micronal AJX 1900). Results were expressed by converting the absorbance of the control to 100% viability.

2.6.4. Protein Content Determination and ALP Assays During MSC Differentiation

The total protein content was calculated in one period, 7 days, to assess whether the biomaterial accelerates the production of cellular proteins or not. This measurement was performed according to the modified method of Lowry [51]. The absorbance was measured spectrophotometrically at 680 nm (Micronal AJX 1900). The alkaline phosphatase (ALP) activity was determined by releasing thymolphthalein by hydrolysis of the thymolphthalein substrate, using a commercial kit according to the manufacturer's instructions (Labtest Diagnóstica), in the same periods of the total protein, using the same lysates. The absorbance was measured in a spectrophotometer (Micronal AJX 1900) at 590 nm.

2.6.5. Formation of Mineralization Nodules

After 12 days of culture, mineralized nodules were observed by staining Alizarin S 2% red (Sigma-Aldrich, St. Louis, Brazil), pH 4.2, and the red dye from Alizarin S stains areas that are rich in calcium. Microplates with the presence of a transwell net (Transwell, Corning/Costar, New York, NY, USA) were used, only for this test. The mineralization nodule formation was observed under an optical microscope (Axio Observer A1, Carl Zeiss, Germany).

2.6.6. Statical Analysis

All tests statistically analyzed were initially submitted to the Kolmogorov-Smirnov normality test and homogeneity of the results was observed ($p > 0.05$). Data from the mechanical assay were analyzed by one-factor ANOVA ($p < 0.05$) and Tukey's posthoc test. Data from *in vitro* tests were analyzed by two-factor ANOVA ($p < 0.05$), considering the period and biomaterial analyzed as variables, and the data are presented as mean value \pm standard deviation. When necessary, they were submitted to Tukey's posthoc test. All tests were performed using the GraphPad Prism 6.0 software (GraphPad Software, San Diego, CA, USA) and for all statistical tests, a significance level of 5% and a power of 80% were adopted.

3. RESULTS AND DISCUSSION

3.1. Rheological Behavior of the β -TCP and β -TCP/S53P4 Inks

To produce a structure with high quality and reproducibility by DIW, the ink must exhibit a continuous flow while printing, presenting a reversible softening behavior under stress, while maintaining its

viscosity between 10 and 100 Pa.s at high shear rates [16,45]. Furthermore, the inks must present yield stress superior to 200 Pa to ensure structural self-support after printing. In the oscillatory regime, the storage modulus (G') must be high and show a decay only after 200 Pa ($\tau_y =$ yield stress), ensuring the sustaining of each printed layer. Associated with these properties, both the viscosity parameter (K) and the shear thinning exponent (n) must be low, so the ink can be easily extruded and recovered after [46].

Figure 1 shows the rheological flow curves of the ceramic inks. Table 1 shows the values of the yield stress (τ_y), viscosity parameter (K), and shear thinning exponent (n), obtained by the adjustment of the Herschel-Bulkley model. The addition of BG S53P4 in the ink resulted in a decrease of the τ_y and the viscosity of the β -TCP/10-S53P4 and β -TCP/20-S53P4 inks when compared with the β -TCP ink. However, there is no difference in the rheological behavior of β -TCP/10-S53P4 and β -TCP/20-S53P4 inks. Every ink formulation showed low viscosity in 100 s^{-1} and yield stress of over 200 Pa and shear-thinning behavior ($n < 1$), which indicates good extrudability and self-support [16, 46].

Table 1: Values of τ_y , K , and n for the Ceramic Inks Adjusted by the Herschel-Bulkley Model

| Composition | τ_y (Pa) | K | n |
|-----------------------|---------------|--------|-------|
| β -TCP | 1685.0 | 2002.0 | 0.068 |
| β -TCP/10-S53P4 | 313.9 | 343.6 | 0.025 |
| β -TCP/20-S53P4 | 195.6 | 259.0 | 0.108 |

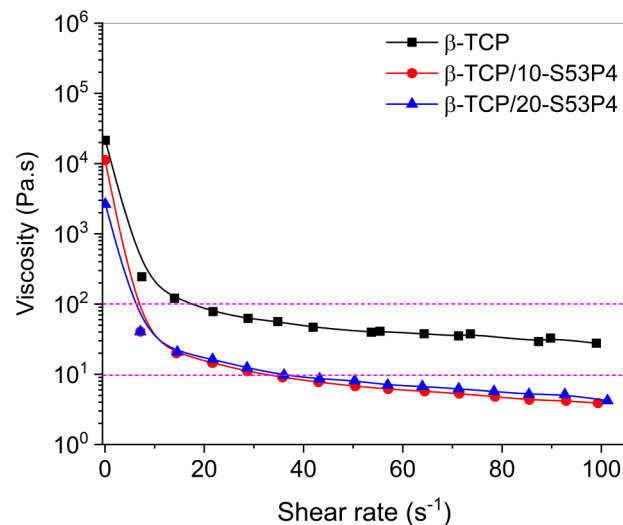


Figure 1: Rheological flow curves for the ceramic inks: dynamic viscosity as a function of the shear rate.

Figure 2 shows the rheological behavior of the inks in the oscillatory analysis. It is possible to notice that the increase of BG S53P4 content (0 to 10% and 10 to 20%) led to a reduction in the crossing point between G' and G'' and lowered G' modulus. This indicates that the addition of BG S53P4 reduces the ink stiffness and, thus, the structural self-support of the scaffolds. The β -TCP/10-S53P4 and β -TCP/20-S53P4 inks maintained high G' (over 10^5 Pa) until 200 Pa, which represents enough stiffness to support the layer stacking of the scaffolds according to Peng *et al.* [16] and Feilden [46]. However, the β -TCP/20-S53P4 ink presented a crossing point lower than 200 Pa, which may lead to structural collapse, depending on the height of the scaffold.

3.2. Physical and Chemical Characterization of the β -TCP and β -TCP/S53P4 Scaffolds

Figure 3 shows the XRD patterns of β -TCP and BG S53P4 powders and the β -TCP and β -TCP/S53P4

(10% and 20% of BG S53P4) scaffold. Regarding the ceramic powders, the analysis demonstrated that the β -TCP powder presents only peaks related to the crystalline phase of β -TCP (β = JCPDS 09-0169), while the BG S53P4 shows a halo between $2\theta = 24^\circ$ and 38° , typical of non-crystalline material. These results confirm that the synthesis and milling parameters were suitable for obtaining the powders without contamination.

Concerning the scaffolds, for β -TCP scaffolds, only the crystalline phase of β -TCP (β = JCPDS 09-0169) was identified. For β -TCP/S53P4, the release of silicon ions led to the formation and stabilization of the crystalline phase of α -TCP (α = JCPDS 009-0348) [34]. Wollastonite (CaSiO_3) (w = JCPDS 027-0088) and high-combeite ($\text{Na}_{15-78}\text{Ca}_3(\text{Si}_6\text{O}_{12})$) (c = JCPDS 001-078-1650) were confirmed in both scaffolds containing BG S53P4. The formation of these phases was expected due to the crystallization of the BG S53P4 during the heat treatment applied at 1150°C [52].

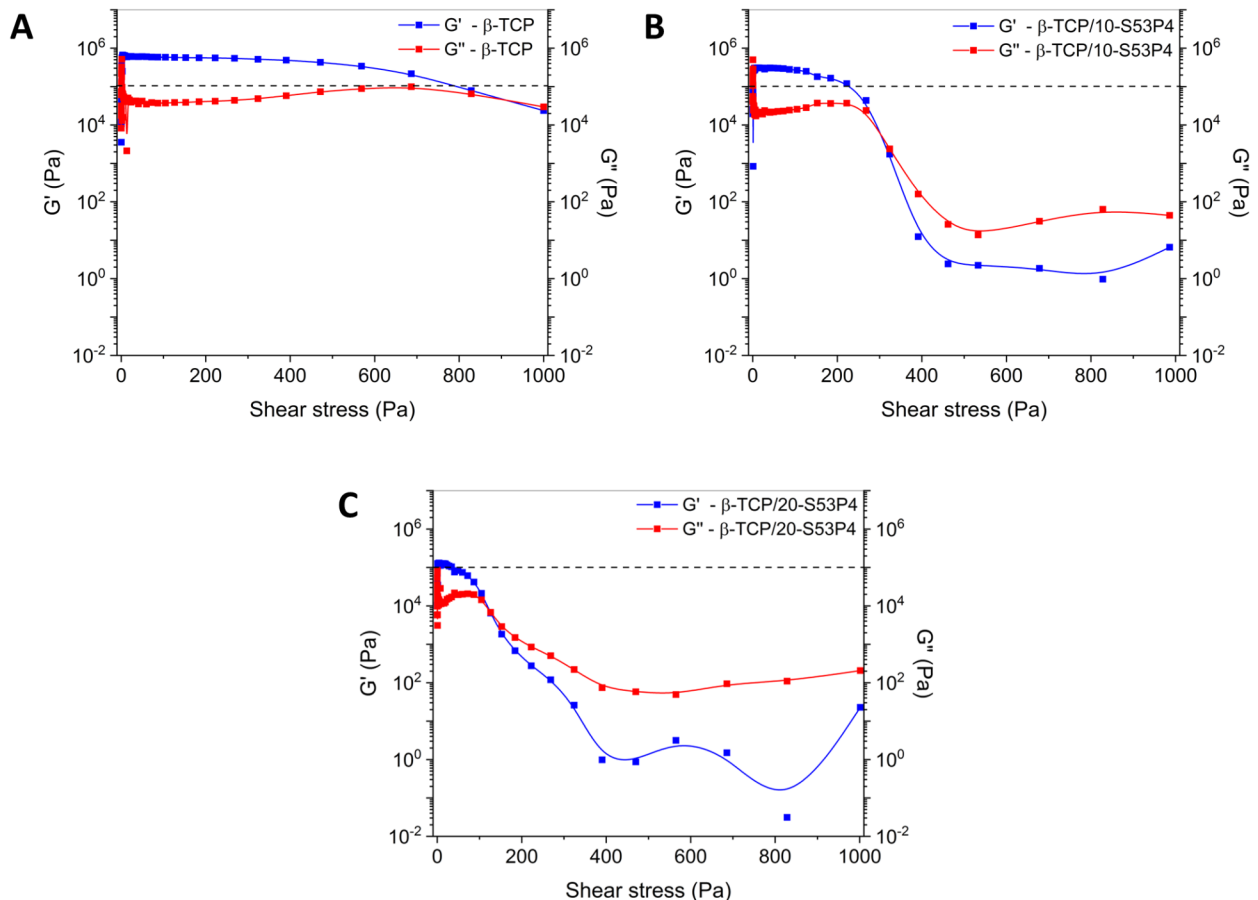


Figure 2: Oscillatory amplitude sweep of the ceramic inks: G' and G'' as a function of shear stress: **A)** β -TCP, **B)** β -TCP/10-S53P4, and **C)** β -TCP/20-S53P4.

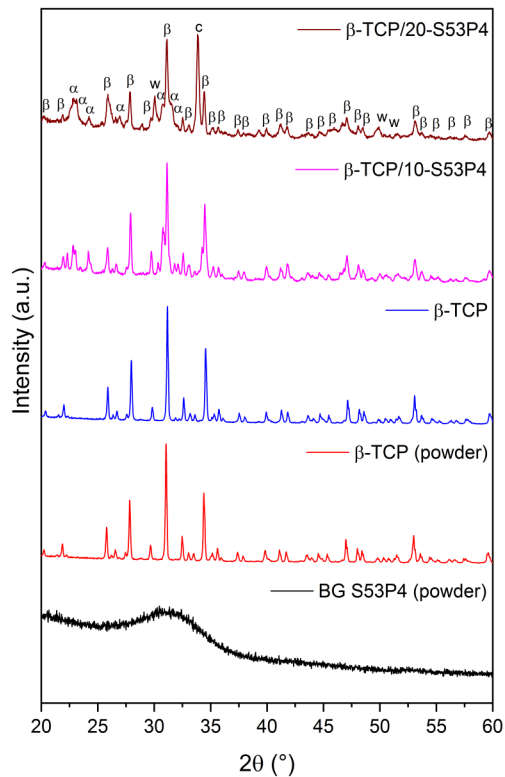


Figure 3: XRD patterns of ceramic powders and β -TCP and β -TCP/BG S53P4 scaffolds.

Figure 4 shows SEM images of the β -TCP and β -TCP/S53P4 scaffolds. All scaffolds presented a regular structure after the printing and sintering process (Figures 4-A1, B1, and C1), corroborating with the rheological results. Also, it is possible to notice that the presence of BG S53P4 in the composition of the β -TCP scaffolds caused a decrease in the microporosity in reason of the formation of the liquid phase during the sintering (Figures 4-A2, A3, B2, B3, C2, and C3). Similar results were found by Ma, Y. *et al* 2019 [35]. They studied β -TCP reinforced with Na_2O - CaO - MgO - P_2O_5 bioglass and found that increasing the amount of bioglass has created a network among the β -TCP particles and decreased the microporosity in the β -TCP matrix [35]. In a recent study from our group [44], the addition of 7.5% (%-wt) of BG S53P4 in β -TCP 3D printed scaffolds have shown a significant decrease in the microporosity of the β -TCP matrix, due to the liquid phase formation of BG S53P4 during the sintering process [44].

Figure 5 shows the elemental mapping of SEM images through EDS and EDS spectra of β -TCP (Figure 5-A), β -TCP/10-S53P4 (Figure 5-B), and β -TCP/20-S53P4 (Figure 5-C) scaffolds. All the scaffolds

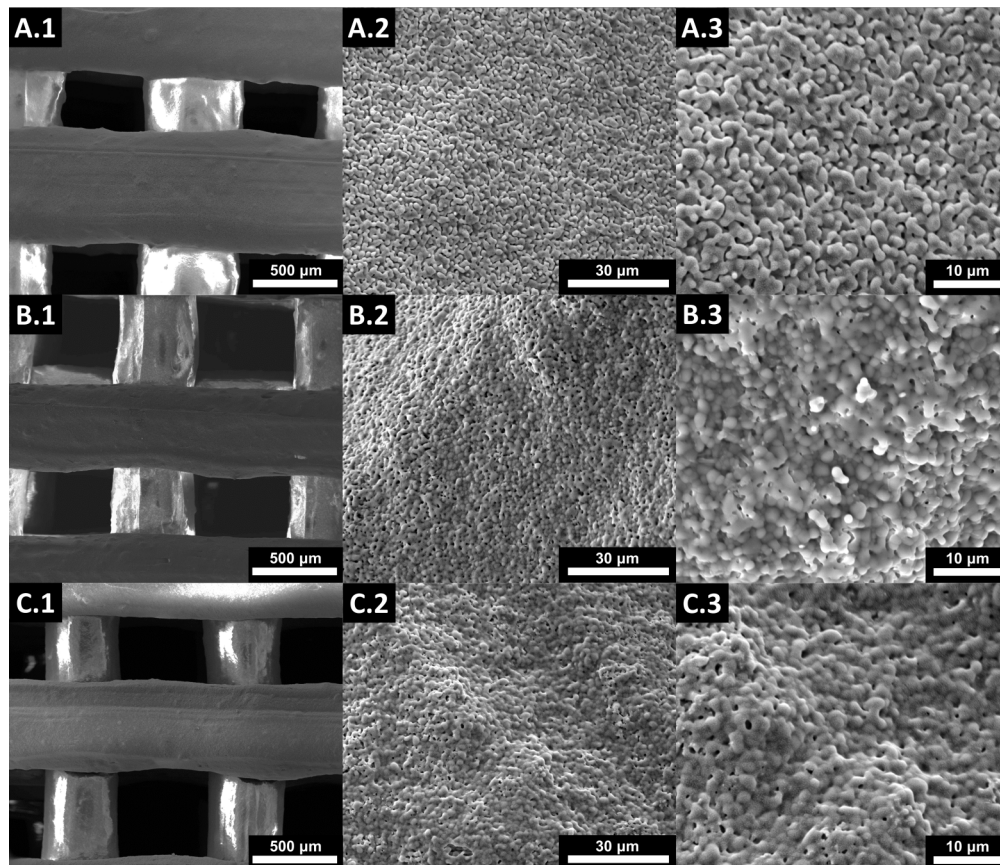


Figure 4: SEM images of the β -TCP (A.1-A.3), β -TCP/10-S53P4 (B.1-B.3), and β -TCP/20-S53P4 (C.1-C.3) scaffolds.

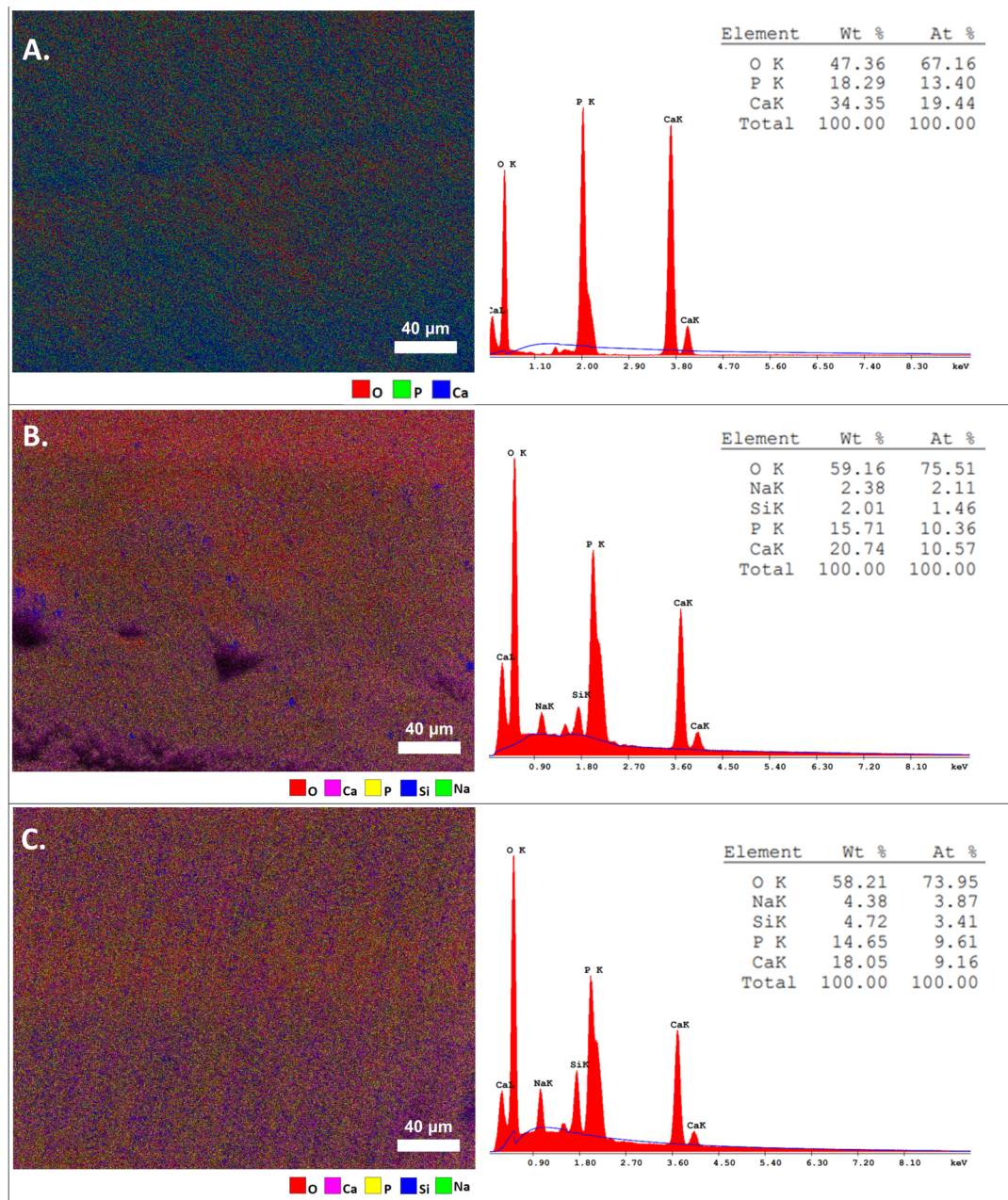


Figure 5: Elemental mapping of SEM images through EDS and EDS spectra of β -TCP (A) and β -TCP/10-S53P4 (B) and β -TCP/20-S53P4 (C) scaffolds.

presented Ca, P, and O elements, common for β -TCP and S53P4 powders. In contrast, Na and Si elements were identified only for the β -TCP/10-S53P3 and β -TCP/20-S53P4 scaffolds because these elements are present in the BG S53P4 composition. The intensity of Na and Si was higher in the β -TCP/20-S53P4 scaffolds that contain a higher amount of BG S53P4. Furthermore, it is possible to note that the elements were homogeneously dispersed in the scaffolds, indicating a good mixture of the powders during the processing.

The values of compressive strength and porosity for the β -TCP and β -TCP/S53P4 scaffolds are shown in Figures 6-A and Figure 6-B, respectively. It is possible to notice that the mean value of compressive strength increased with the addition of BG S53P4 in the scaffolds. The β -TCP scaffolds presented compressive strength of 0.9 ± 0.1 MPa whereas β -TCP/10-S53P4 and β -TCP/20-S53P4 scaffolds presented compressive strength of 1.6 ± 0.6 MPa and 2.1 ± 0.9 MPa, respectively. There was a significant difference between the β -TCP and β -TCP/20-S53P4 scaffolds, and between the β -TCP/10-S53P4 and β -TCP/20-

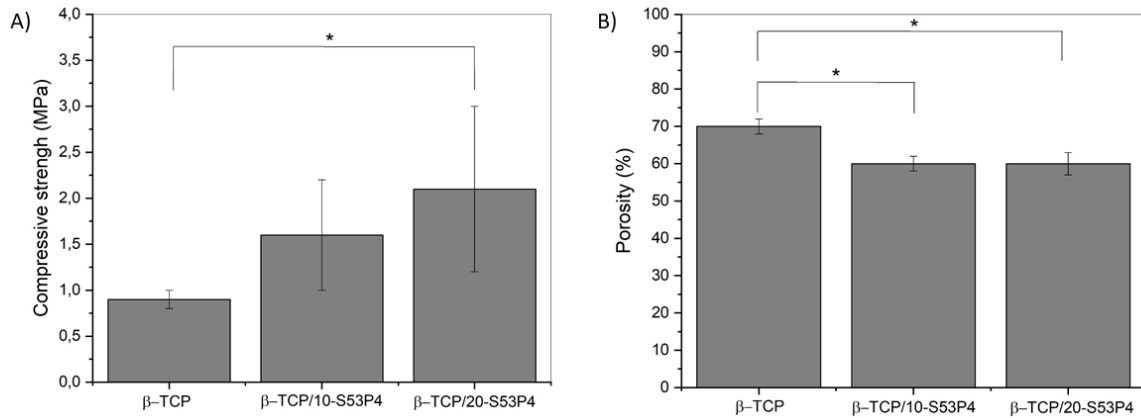


Figure 6: Mechanical properties of the scaffolds: compressive strength (mean \pm SD, $n = 7$, $*p < 0.05$) (A), and porosity curves (mean \pm SD, $n = 7$, $*p < 0.05$) (B).

S53P4, proving that the increase of the BG amount improves the mechanical resistance. The total porosity decreased from $70 \pm 2\%$ in the β -TCP scaffolds to $60 \pm 2\%$ in the β -TCP/10-S53P4 scaffolds and $60 \pm 3\%$ in the β -TCP/20-S53P4 scaffolds. There was a significant difference between β -TCP and β -TCP/S53P4 scaffolds (β -TCP/10-S53P4 and β -TCP/20-S53P4), however, there was no significant difference between β -TCP/10-S53P4 and β -TCP/20-S53P4. The presence of BG S53P4 in the composition led to the formation of a liquid phase which filled the microporosity of the scaffolds, causing a decrease in the total porosity and enhancing the mechanical strength [44]. Baino *et al.* 2020 reported that the scaffolds of β -TCP and CEL2 bioactive glass based on $45\text{SiO}_2\text{-}3\text{P}_2\text{O}_5\text{-}26\text{CaO}\text{-}7\text{MgO}\text{-}15\text{Na}_2\text{O}\text{-}4\text{K}_2\text{O}$ mol.% (3% - wt) obtained by the foam replica reached more mechanical stability and enhanced mechanical properties [53]. The β -TCP scaffolds containing the CEL2 bioactive glass showed 0.14 ± 0.07 MPa, reaching the range of the cancellous bone (0.1 - 10 MPa) [53].

Regarding the absence of difference in the porosity over the two compositions with BG S53P4, it can be attributed to a higher shrinkage and more compaction in the internal structure. Similar results were found by Ma *et al.* 2019 with 3D printed β -TCP scaffolds reinforced with $\text{Na}_2\text{O}\text{-}\text{CaO}\text{-}\text{MgO}\text{-}\text{P}_2\text{O}_5$ bioglass in the amount of 20% (%-wt) [35]. The scaffolds were obtained with a cubic shape, 60% of porosity, and reached 8.34 MPa of compressive strength [35]. Zhu *et al.* 2021 reached higher mechanical properties in 3D printed scaffolds based on β -TCP reinforced with $\text{Na}_2\text{O}\text{-}\text{CaO}\text{-}\text{MgO}\text{-}\text{P}_2\text{O}_5$ bioactive glass in comparison with the traditional bone graft produced by the foaming

method [54]. Li *et al.* 2021 studied 3D printed scaffolds based on β -TCP containing 58S bioactive glass and reached a comprehensive strength of 11 ± 0.4 MPa, with a slurry with 60% of solids (%-wt) [55]. In conclusion, the results obtained in this work are according to the literature, showing that the increase of the bioactive glass contents leads to enhancing the scaffolds' mechanical properties.

3.3. Apatite Mineralization Ability of the β -TCP and β -TCP/S53P4 Scaffolds

Figure 7 shows the XRD patterns for β -TCP and β -TCP/S53P4 scaffolds soaked in SBF after 7 and 14 days. The XRD patterns of β -TCP scaffolds presented peaks relate to the β -TCP phase (JCPDS: 09-0169) in the majority and some peaks indicating a low formation of hydroxyapatite (JCPDS: 09-0432). β -TCP/10-S53P4 and β -TCP/20-S53P4 XRD patterns presented a higher formation of hydroxyapatite and α -TCP (JCPDS: 09-0348) phases. The α -TCP phase formation was also reported by previous studies of our group [44] and it can be correlated with Si ions that can reduce the phase transformation temperature of β -TCP α -TCP [44]. In addition, it was noticed that the addition of BG S53P4 increases the hydroxyapatite formation. It is known that the presence of Si ions from BG S53P4 in calcium phosphates materials facilitates the hydroxyapatite formation in the scaffold surface [56]. Pietak *et al.* 2007 studied the substitution of Si ions in calcium phosphate materials and found that Si ions have facilitated the obtention of hydroxyapatite on the calcium phosphate surface and increased their biological activity [57]. Comparing the XRD patterns of β -TCP/10-S53P4 and β -TCP/20-S53P4 it can be noticed a higher hydroxyapatite formation is found in β -

TCP/10-S53P4. This could be explained by a higher intensity of peaks related to the α -TCP phase in the β -TCP/20-S53P4, due to the Si ions inducing the phase transformation, which could overlap the hydroxyapatite peaks. However, by SEM images it can be noticed that β -TCP/20-S53P4 scaffold shows more hydroxyapatite on the surface than β -TCP/10-S53P4 (Figure 8), as was expected due to the higher amount of S53P4 and Si ions. β -TCP scaffolds showed poor hydroxyapatite formation on the surface. The shape of hydroxyapatite on the scaffolds' surface and the formation in clusters corroborates with other studies in the literature [58-61].

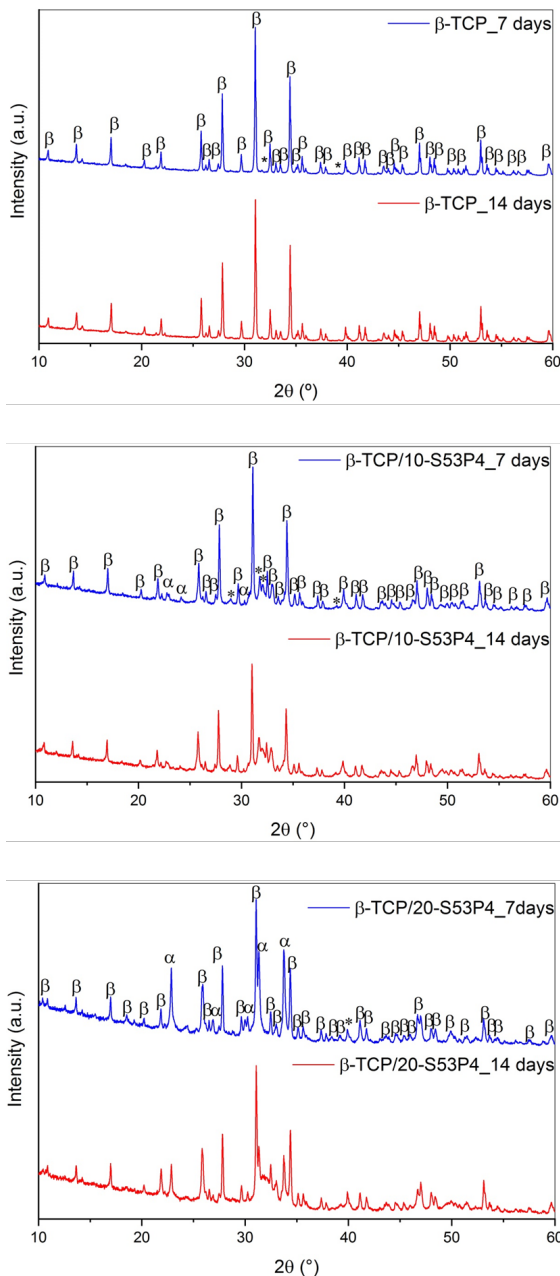


Figure 7: XRD patterns of β -TCP, β -TCP/10-S53P4, and β -TCP/20-S53P4 scaffolds soaked in SBF after 7 and 14 days.

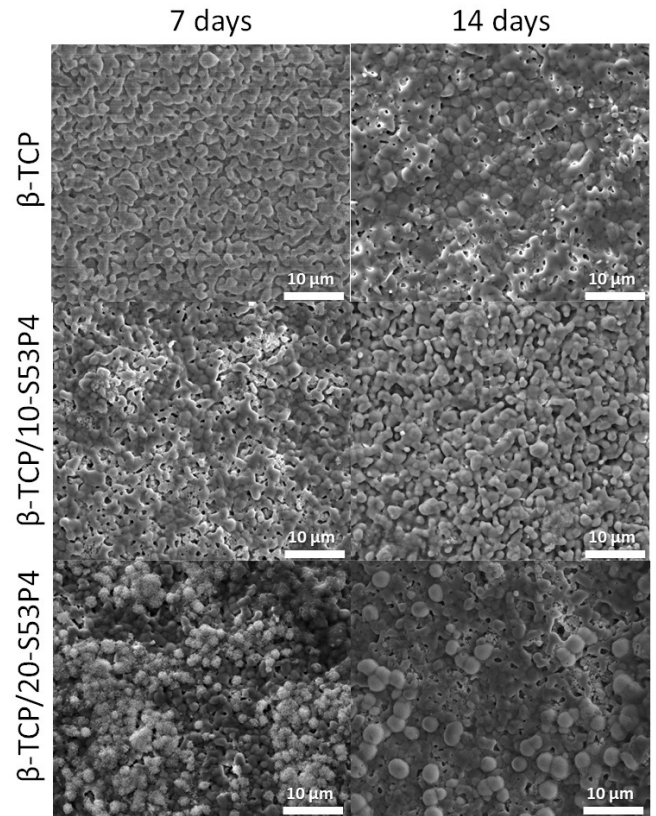


Figure 8: Surface morphology of β -TCP, β -TCP/10-S53P4, and β -TCP/20-S53P4 scaffolds, by SEM, after 7 and 14 days in SBF.

3.4. *In vitro* Biological Assays

After 5 days of culture, the scaffolds were analyzed by scanning electron microscopy (SEM) (Figure 9) to show the cellular interaction on the β -TCP (Figure 9-A), β -TCP/10-S53P4 (Figure 9-B), and β -TCP/20-S53P4 (Figure 9-C) scaffolds. In this analysis, it was evidenced that all scaffolds allowed cellular dissemination. It was possible to observe that the cells penetrated these pores, permeating their porous structure.

Regarding cell viability, the β -TCP/10-S53P4 scaffolds had the highest mean value of viable cells, however, there was no statistical difference with the other compositions ($p > 0.05$), as shown in Figure 10-A. It is known that bioactive glasses release ions capable of increasing the ambient pH, and this increase, although good for the promotion of antimicrobial activity, can also be detrimental to cell survival [62]. This study showed that the β -TCP, β -TCP/10-S53P4, and β -TCP/20-S53P4 scaffolds did not exhibit toxicity to the cells. Despite without significant difference, the β -TCP/10-S53P4 favored cell growth. As in our study,

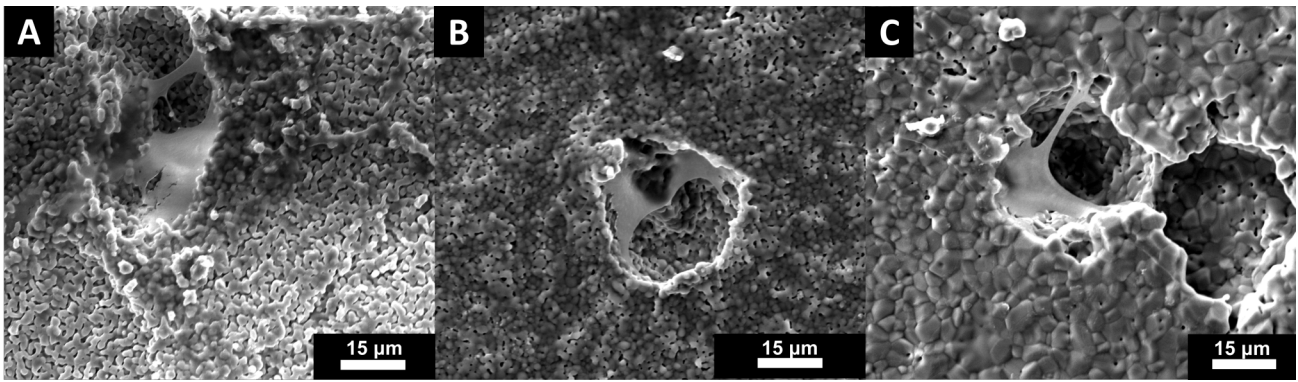


Figure 9: SEM images of cells adherent on the β -TCP (A), β -TCP/10-S53P4 (B), and β -TCP/20-S53P4 (C) scaffolds.

the study by Waselau *et al.* [63] also observed cell growth in samples that contained BG S53P4 compared to the group with only β -TCP.

Regarding cellular metabolic activity, the total amount of protein produced by cells in contact with the scaffold was evaluated. It is possible to observe that all compositions exhibited a higher value than the control group, however, no composition presented a statistical difference when compared to each other ($p < 0.05$), as shown in Figure 10-B. The previous analysis of total protein is one of the biochemical assays that allow to measure whether osteogenesis is occurring, so both the measurement of total protein content and alkaline phosphatase activity are predictive methods for the formation of mineralized matrix [64]. In addition, ALP is an essential marker in the differentiation of mesenchymal cells into osteoblasts [65-66]. Thus, the amount of ALP in the environment increases, which means that differentiation is taking place and consequently the osteogenesis process will take place [67].

There were no statistically significant differences between the scaffolds analyzed ($p > 0.05$). However, β -TCP/10-S53P4 scaffolds presented the highest mean value among the other compositions with β -TCP and β -TCP/20-S53P4, as shown in Figure 10-C. Those results agree with the study of Ojansivu *et al.* 2018 [68] who also did not observe greater expression of ALP in the experimental groups.

The formation of mineralization nodules was performed within 12 days of cell culture. The formation of calcium mineralization nodules is an indication that the process of osteoblastic cell differentiation is taking place [67]. Thus, when cells are stained with alizarin red, the dye will bind to calcium present in the newly formed nodules, producing the red spots observed in Figure 11. It was observed that in all scaffolds there was the presence of these nodules, indicating the final differentiation of MSC in osteoblastic cells, results similar to Vallittu *et al.* [69] that also verified that BG S53P4 ions in its composition are capable of favoring osteogenic differentiation.

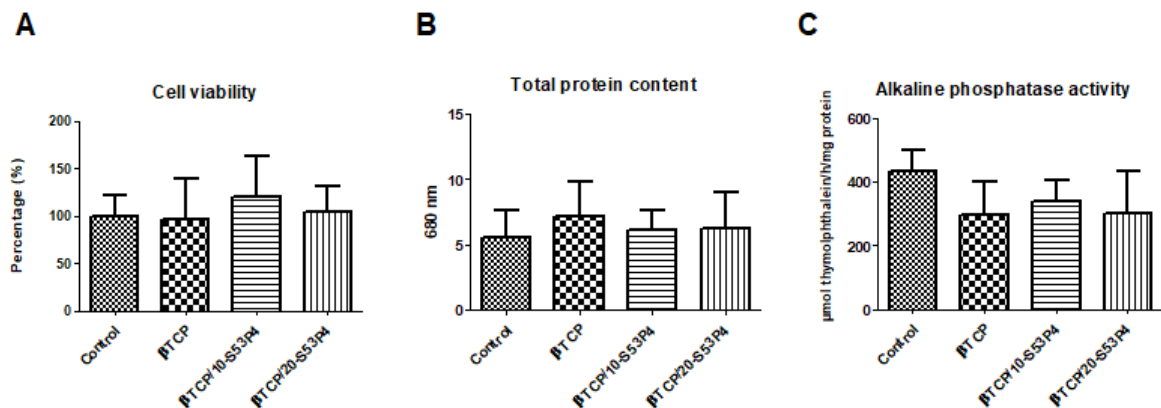


Figure 10: *In vitro* tests: graphics represent mean values (\pm) standard deviation Cell viability (Percentage %) after seven days (A). Total protein content (OD- 690 nm) after seven days (B). Alkaline phosphatase activity (OD- 580 nm) after seven days (C).

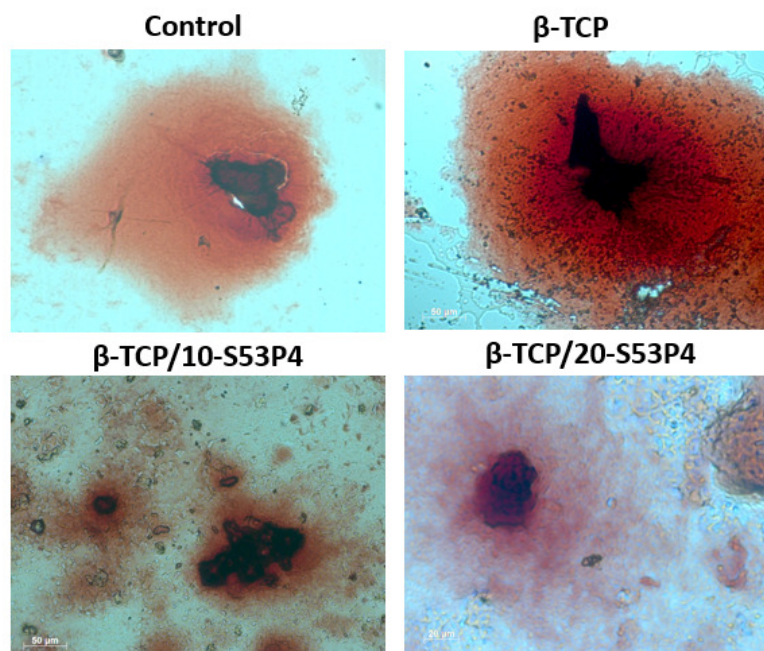


Figure 11: Mineralization nodules after 12 days. Images of the formation of mineralization nodules. Cells were stained with Red Alizarin S to visualize formed calcium deposits. Original magnification $\times 50$ (scale bars = 50 μm).

4. CONCLUSION

The study successfully utilized the DIW technique to produce 3D-printed scaffolds of β -TCP and β -TCP/S53P4. *In vitro* biological assessments revealed that scaffolds exhibited favorable pre-osteoblastic cell growth characteristics. Thus, this research presented a feasible approach for obtaining scaffolds with desirable properties for bone regeneration. It was found that the addition of BG S53P4 to β -TCP scaffolds improved their mechanical properties and mineralization in SBF. In conclusion, the results showed in this research present an alternative to bone treatment through the production of substitutes for traditional grafts.

HIGHLIGHTS

- Additive manufacturing based on material extrusion was used to print the β -TCP and β -TCP/S53P4 scaffolds.
- All the ceramic inks were adjusted by Herschel–Bulkley model and presented pseudoplastic behavior.
- The BG S53P4 addition decreased the porosity of the scaffold and increased its compression strength.
- The β -TCP and β -TCP/S53P4 scaffolds presented viability of MSC cells, total protein content, and ALP activity.

- All the scaffolds presented the formation of calcium-mineralized nodules, indicating the differentiation of MSC into osteoblastic cells.

ACKNOWLEDGMENTS

This project was funded by Brazilian agencies São Paulo Research Foundation (FAPESP, Grant IDs: 2019/08141-9, 2019/19187-0, 2021/14593-0, and 2019/19594-4) and Coordenação de Aperfeiçoamento de Pessoal de Nível Superior – Brasil (CAPES) – Finance Code 001. The authors would like to thank the NAPCEM Multi-User Laboratory (UNIFESP) for the facilities.

DECLARATION OF COMPETING INTEREST

The authors declare that they have no known competing financial interests or personal relationships that could have appeared to influence the work reported in this paper.

CREDIT AUTHORSHIP CONTRIBUTION STATEMENT

Ana Paula Nogueira Alves: Methodology, Investigation, Writing – original draft. **Lucas Barbosa:** Methodology, Investigation, Formal Analysis, Writing – original draft. **Rodrigo L. M. S. Oliveira:** Methodology, Investigation, Formal analysis, Writing – original draft. **Julia Andrade de Oliveira:** Methodology, Investigation. **Mariana de Sá Alves:** Methodology,

Investigation, Formal analysis. **Luna Marotta Reis de Vasconcellos**: Supervision, Review and Editing. **Eliandra de Sousa Trichês**: Supervision, Resources, Review, and Editing.

REFERENCES

- [1] H.C. Pape, A. Evans, P. Kobbe, Autologous Bone Graft: Properties and Techniques, 24 (2010) 36-40. <https://doi.org/10.1097/BOT.0b013e3181ce4a1>
- [2] A.H. Schmidt, Autologous bone graft: Is it still the gold standard?, *Injury*. (2021) 1-5. <https://doi.org/10.1016/j.injury.2021.01.043>
- [3] W. Wang, K.W.K. Yeung, Bone grafts and biomaterials substitutes for bone defect repair: A review, *Bioact. Mater.* 2 (2017) 224-247. <https://doi.org/10.1016/j.bioactmat.2017.05.007>
- [4] L. Vidal, C. Kamleitner, M. Brennan, A. Hoornaert, P. Layrolle, Reconstruction of Large Skeletal Defects: Current Clinical Therapeutic Strategies and Future Directions Using 3D Printing, *Front. Bioeng. Biotechnol.* 8 (2020). <https://doi.org/10.3389/fbioe.2020.00061>
- [5] T. Winkler, F.A. Sass, G.N. Duda, K. Schmidt-Bleek, A review of biomaterials in bone defect healing, remaining shortcomings and future opportunities for bone tissue engineering: The unsolved challenge, *Bone Jt. Res.* 7 (2018) 232-243. <https://doi.org/10.1302/2046-3758.73.BJR-2017-0270.R1>
- [6] G. Brunello, S. Panda, L. Schiavon, S. Sivoletta, L. Biasetto, M. Del Fabbro, The impact of bioceramic scaffolds on bone regeneration in preclinical in vivo studies: A systematic review, *Materials (Basel)*. 13 (2020) 1-26. <https://doi.org/10.3390/ma13071500>
- [7] K. Lin, R. Sheikh, S. Romanazzo, I. Roohani, 3D printing of bioceramic scaffolds-barriers to the clinical translation: From promise to reality, and future perspectives, *Materials (Basel)*. 12 (2019). <https://doi.org/10.3390/ma12172660>
- [8] F. Baino, G. Novajra, C. Vitale-Brovarone, Bioceramics and scaffolds: A winning combination for tissue engineering, *Front. Bioeng. Biotechnol.* 3 (2015) 1-17. <https://doi.org/10.3389/fbioe.2015.00202>
- [9] H. Jodati, B. Yilmaz, Z. Evis, A review of bioceramic porous scaffolds for hard tissue applications: Effects of structural features, *Ceram. Int.* 46 (2020) 15725-15739. <https://doi.org/10.1016/j.ceramint.2020.03.192>
- [10] M.V. Varma, B. Kandasubramanian, S.M. Ibrahim, 3D printed scaffolds for biomedical applications, *Mater. Chem. Phys.* 255 (2020) 123642. <https://doi.org/10.1016/j.matchemphys.2020.123642>
- [11] R. Galante, C.G. Figueiredo-Pina, A.P. Serro, Additive manufacturing of ceramics for dental applications: A review, *Dent. Mater.* 35 (2019) 825-846. <https://doi.org/10.1016/j.dental.2019.02.026>
- [12] Y. Yang, G. Wang, H. Liang, C. Gao, S. Peng, L. Shen, C. Shuai, Additive manufacturing of bone scaffolds, *Int. J. Bioprinting.* 5 (2019) 1-25. <https://doi.org/10.18063/ijb.v5i1.148>
- [13] X. Zhou, Y. Feng, J. Zhang, Y. Shi, L. Wang, Recent advances in additive manufacturing technology for bone tissue engineering scaffolds, *Int. J. Adv. Manuf. Technol.* 108 (2020) 3591-3606. <https://doi.org/10.1007/s00170-020-05444-1>
- [14] Y. Chen, W. Li, C. Zhang, Z. Wu, J. Liu, Recent Developments of Biomaterials for Additive Manufacturing of Bone Scaffolds, *Adv. Healthc. Mater.* 9 (2020) 1-28. <https://doi.org/10.11648/j.am.20200901.11>
- [15] C. Garot, G. Bettega, C. Picart, Additive Manufacturing of Material Scaffolds for Bone Regeneration: Toward Application in the Clinics, *Adv. Funct. Mater.* 31 (2021) 1-17. <https://doi.org/10.1002/adfm.202006967>
- [16] E. Peng, D. Zhang, J. Ding, Ceramic Robocasting: Recent Achievements, Potential, and Future Developments, *Adv. Mater.* 30 (2018) 1-14. <https://doi.org/10.1002/adma.201802404>
- [17] U. Golcha, A.S. Praveen, D.L. Belgin Paul, Direct ink writing of ceramics for bio medical applications - A Review, *IOP Conf. Ser. Mater. Sci. Eng.* 912 (2020). <https://doi.org/10.1088/1757-899X/912/3/032041>
- [18] M. Ginebra, Rheological characterisation of ceramic inks for 3D direct ink writing: A review, *J. Eur. Ceram. Soc.* (2021).
- [19] J.H. Shepherd, S.M. Best, Calcium phosphate scaffolds for bone repair, *Jom.* 63 (2011) 83-92. <https://doi.org/10.1007/s11837-011-0063-9>
- [20] Q. Liu, W.F. Lu, W. Zhai, Toward stronger robocast calcium phosphate scaffolds for bone tissue engineering: A mini-review and meta-analysis, *Mater. Sci. Eng. C.* (2021) 112578. <https://doi.org/10.1016/j.msec.2021.112578>
- [21] H. Ma, C. Feng, J. Chang, C. Wu, 3D-printed bioceramic scaffolds: From bone tissue engineering to tumor therapy, *Acta Biomater.* 79 (2018) 37-59. <https://doi.org/10.1016/j.actbio.2018.08.026>
- [22] N. Eliaz, N. Metoki, Calcium phosphate bioceramics: A review of their history, structure, properties, coating technologies and biomedical applications, *Materials (Basel)*. 10 (2017). <https://doi.org/10.3390/ma10040334>
- [23] A. Boskey, Bone mineral crystal size., *Osteoporos. Int.* 14 Suppl 5 (2003) 16-21. <https://doi.org/10.1007/s00198-003-1468-2>
- [24] R.Z. Legeros, J.P. Legeros, Hydroxyapatite, *Bioceram. Their Clin. Appl.* (2008) 367-394. <https://doi.org/10.1533/9781845694227.2.367>
- [25] C. Rey, C. Combes, C. Drouet, M.J. Glimcher, Bone mineral: Update on chemical composition and structure, *Osteoporos. Int.* 20 (2009) 1013-1021. <https://doi.org/10.1007/s00198-009-0860-y>
- [26] J. Jeong, J.H. Kim, J.H. Shim, N.S. Hwang, C.Y. Heo, Bioactive calcium phosphate materials and applications in bone regeneration, *Biomater. Res.* 23 (2019) 1-11. <https://doi.org/10.1186/s40824-018-0153-7>
- [27] J. Lu, H. Yu, C. Chen, Biological properties of calcium phosphate biomaterials for bone repair: a review, *RSC Adv.* (2018) 2015-2033. <https://doi.org/10.1039/C7RA11278E>
- [28] Z.F. Chen, B.W. Darvell, V.W.H. Leung, Hydroxyapatite solubility in simple inorganic solutions, *Arch. Oral Biol.* 49 (2004) 359-367. <https://doi.org/10.1016/j.archoralbio.2003.12.004>
- [29] S. Yamada, D. Heymann, J.M. Boulter, G. Daculsi, Osteoclastic resorption of calcium phosphate ceramics with different hydroxyapatite/ β -tricalcium phosphate ratios, *Biomaterials.* 18 (1997) 1037-1041. [https://doi.org/10.1016/S0142-9612\(97\)00036-7](https://doi.org/10.1016/S0142-9612(97)00036-7)
- [30] M. Bohner, B.L.G. Santoni, N. Döbelin, β -tricalcium phosphate for bone substitution: Synthesis and properties, *Acta Biomater.* 113 (2020) 23-41. <https://doi.org/10.1016/j.actbio.2020.06.022>
- [31] R. Al Jasser, A. AlSubaie, F. AlShehri, Effectiveness of beta-tricalcium phosphate in comparison with other materials in treating periodontal infra-bony defects around natural teeth: a systematic review and meta-analysis, *BMC Oral Health.* 21 (2021) 1-14. <https://doi.org/10.1186/s12903-021-01570-8>

- [32] E. Champion, Sintering of calcium phosphate bioceramics, *Acta Biomater.* 9 (2013) 5855-5875.
<https://doi.org/10.1016/j.actbio.2012.11.029>
- [33] H.S. Ryu, H.J. Youn, K. Sun Hong, B.S. Chang, C.K. Lee, S.S. Chung, An improvement in sintering property of β -tricalcium phosphate by addition of calcium pyrophosphate, *Biomaterials.* 23 (2002) 909-914.
[https://doi.org/10.1016/S0142-9612\(01\)00201-0](https://doi.org/10.1016/S0142-9612(01)00201-0)
- [34] J.H. Lopes, J.A. Magalhães, R.F. Gouveia, C.A. Bertran, M. Motisuke, S.E.A. Camargo, E. de S. Trichês, Hierarchical structures of β -TCP/45S5 bioglass hybrid scaffolds prepared by gelcasting, *J. Mech. Behav. Biomed. Mater.* 62 (2016) 10-23.
<https://doi.org/10.1016/j.jmbbm.2016.04.028>
- [35] Y. Ma, H. Dai, X. Huang, Y. Long, 3D printing of bioglass-reinforced β -TCP porous bioceramic scaffolds, *J. Mater. Sci.* 54 (2019) 10437-10446.
<https://doi.org/10.1007/s10853-019-03632-3>
- [36] S.B. Hua, J. Su, Z.L. Deng, J.M. Wu, L.J. Cheng, X. Yuan, F. Chen, H. Zhu, D.H. Qi, J. Xiao, Y.S. Shi, Microstructures and properties of 45S5 bioglass® & BCP bioceramic scaffolds fabricated by digital light processing.pdf, *Addit. Manuf.* 45 (2021) 102074.
<https://doi.org/10.1016/j.addma.2021.102074>
- [37] L.L. Hench, The story of Bioglass®, *J. Mater. Sci. Mater. Med.* 17 (2006) 967-978.
<https://doi.org/10.1007/s10856-006-0432-z>
- [38] D.C. Greenspan, Glass, and Medicine: The Larry Hench Story, *Int. J. Appl. Glas. Sci.* 7 (2016).
<https://doi.org/10.1111/ijag.12204>
- [39] J.R. Jones, Reprint of Review of bioactive glass: From Hench to hybrids, *Acta Biomater.* 23 (2015) S53-S82.
<https://doi.org/10.1016/j.actbio.2015.07.019>
- [40] F. Baino, S. Hamzehlou, S. Kargozar, Bioactive glasses: Where are we and where are we going?, *J. Funct. Biomater.* 9 (2018).
<https://doi.org/10.3390/jfb9010025>
- [41] L.L. Hench, Some comments on bioglass: Four eras of discovery and development, *Biomed. Glas.* 1 (2015).
<https://doi.org/10.1515/bglass-2015-0001>
- [42] J.R. Jones, D.S. Brauer, L. Hupa, D.C. Greenspan, Bioglass and Bioactive Glasses and Their Impact on Healthcare, *Int. J. Appl. Glas. Sci.* 7 (2016) 423-434.
<https://doi.org/10.1111/ijag.12252>
- [43] N.A.P. Van Gestel, J. Geurts, D.J.W. Hulsen, B. Van Rietbergen, S. Hofmann, J.J. Arts, Clinical Applications of S53P4 Bioactive Glass in Bone Healing and Osteomyelitis Treatment: A Literature Review, *Biomed Res. Int.* (2015).
<https://doi.org/10.1155/2015/684826>
- [44] A.P.N. Alves, M. Arango-Ospina, R.L.M.S. Oliveira, I.M. Ferreira, E.G. de Moraes, M. Hartmann, A.P.N. de Oliveira, A.R. Boccaccini, E. de Sousa Trichês, 3D-printed β -TCP/S53P4 bioactive glass scaffolds coated with tea tree oil: Coating optimization, in vitro bioactivity and antibacterial properties, *J. Biomed. Mater. Res. - Part B Appl. Biomater.* (2022) 1-14.
- [45] R.L.M.S. Oliveira, A.P.N. Alves, L. Barbosa, A.P. Silva, G.L. de Cena, K. Conceição, D.B. Tada, E. de S. Trichês, 3D printing of bioactive glass S53P4/sodium alginate sintering-free scaffolds, *Bioprinting.* 27 (2022).
<https://doi.org/10.1016/j.bprint.2022.e00226>
- [46] E. Feilden, E.G.T. Blanca, F. Giuliani, E. Saiz, L. Vandeperre, Robocasting of structural ceramic parts with hydrogel inks, *J. Eur. Ceram. Soc.* 36 (2016) 2525-2533.
<https://doi.org/10.1016/j.jeurceramsoc.2016.03.001>
- [47] T. Kokubo, H. Kushitani, S. Sakka, T. Kitsugi, T. Yamamuro, Solutions able to reproduce in vivo surface-structure changes in bioactive glass-ceramic A-W3, *J. Biomed. Mater. Res.* 24 (1990) 721-734.
<https://doi.org/10.1002/jbm.820240607>
- [48] T. Kokubo, H. Takadama, How useful is SBF in predicting in vivo bone bioactivity?, *Biomaterials.* 27 (2006) 2907-2915.
<https://doi.org/10.1016/j.biomaterials.2006.01.017>
- [49] D. de C.R. Mello, L.M. Rodrigues, F.Z.D. Mello, T.F. Gonçalves, B. Ferreira, S.G. Schneider, L.D. de Oliveira, L.M.R. de Vasconcellos, Biological and microbiological interactions of Ti-35Nb-7Zr alloy and its basic elements on bone marrow stromal cells: good prospects for bone tissue engineering, *Int. J. Implant Dent.* 6 (2020).
<https://doi.org/10.1186/s40729-020-00261-3>
- [50] ISO 10993-5:2009(en), Biological evaluation of medical devices - Part 5: Tests for in vitro cytotoxicity, (n.d.).
- [51] O.H. Lowry, N.J. Rosebrough, A.L. Farr, R.J. Randall, Protein Measurement with the Folin Phenol Reagent*, (1951).
[https://doi.org/10.1016/S0021-9258\(19\)52451-6](https://doi.org/10.1016/S0021-9258(19)52451-6)
- [52] B.R. Spirandeli, T.M.B. Campos, R.G. Ribas, G.P. Thim, E. de S. Trichês, Evaluation of colloidal and polymeric routes in sol-gel synthesis of a bioactive glass-ceramic derived from 45S5 bioglass, *Ceram. Int.* 46 (2020) 20264-20271.
<https://doi.org/10.1016/j.ceramint.2020.05.108>
- [53] F. Baino, S. Caddeo, C. Vitale-brovarone, Sintering effects of bioactive glass incorporation in tricalcium phosphate scaffolds - Journal Pre-proofs, *Mater. Lett.* 274 (2020) 128010.
<https://doi.org/10.1016/j.matlet.2020.128010>
- [54] H. Zhu, M. Li, X. Huang, D. Qi, L.P. Nogueira, X. Yuan, W. Liu, Z. Lei, J. Jiang, H. Dai, J. Xiao, 3D printed tricalcium phosphate-bioglass scaffold with gyroid structure enhance bone ingrowth in challenging bone defect treatment, *Appl. Mater. Today.* 25 (2021).
<https://doi.org/10.1016/j.apmt.2021.101166>
- [55] X. Li, H. Zhang, Y. Shen, Y. Xiong, L. Dong, J. Zheng, S. Zhao, Fabrication of porous β -TCP/58S bioglass scaffolds via top-down DLP printing with high solid loading ceramic-resin slurry, *Mater. Chem. Phys.* 267 (2021).
<https://doi.org/10.1016/j.matchemphys.2021.124587>
- [56] P.A. Forero-Sossa, J.D. Salazar-Martinez, V.J. Barajas-Aguilar, I.U. Olvera-Alvarez, J. Henao, D.G. Espinosa-Arbelaez, G. Trápaga-Martínez, A.L. Giraldo-Betancur, Effect of S53P4 bioactive glass content on structural and in-vitro behavior of hydroxyapatite/bioactive glass mixtures prepared by mechanical milling, *Ceram. Int.* 49 (2022) 4322-4330.
<https://doi.org/10.1016/j.ceramint.2022.09.317>
- [57] A.M. Pietak, J.W. Reid, M.J. Stott, M. Sayer, Silicon substitution in the calcium phosphate bioceramics, *Biomaterials.* 28 (2007) 4023-4032.
<https://doi.org/10.1016/j.biomaterials.2007.05.003>
- [58] C. Shuai, W. Yang, P. Feng, S. Peng, H. Pan, Accelerated degradation of HAP/PLLA bone scaffold by PGA blending facilitates bioactivity and osteoconductivity, *Bioact Mater.* 6 (2021) 490-502.
<https://doi.org/10.1016/j.bioactmat.2020.09.001>
- [59] P. Feng, P. Wu, C. Gao, Y. Yang, W. Guo, W. Yang, C. Shuai, A Multimaterial Scaffold With Tunable Properties: Toward Bone Tissue Repair, *Advanced Science.* 5 (2018).
<https://doi.org/10.1002/adv.201700817>
- [60] P. Feng, K. Wang, Y. Shuai, S. Peng, Y. Hu, C. Shuai, Hydroxyapatite nanoparticles in situ grown on carbon nanotube as a reinforcement for poly (ϵ -caprolactone) bone scaffold, *Mater Today Adv.* 15 (2022).
<https://doi.org/10.1016/j.mtadv.2022.100272>
- [61] C. Shuai, B. Peng, P. Feng, L. Yu, R. Lai, A. Min, In situ synthesis of hydroxyapatite nanorods on graphene oxide nanosheets and their reinforcement in biopolymer scaffold, *J Adv Res.* 35 (2022) 13-24.
<https://doi.org/10.1016/j.jare.2021.03.009>
- [62] J. Sarin, M. Vuorenmaa, P.K. Vallittu, R. Grénman, P. Boström, P. Riihilä, L. Nissinen, V.M. Kähäri, J. Pulkkinen,

- The Viability and Growth of HaCaT Cells After Exposure to Bioactive Glass S53P4-Containing Cell Culture Media, *Otol. Neurotol.* 42 (2021) e559-e567.
<https://doi.org/10.1097/MAO.0000000000003057>
- [63] M. Waselau, M. Patrikoski, B. Mannerström, M. Raki, K.A. Bergstroem, B. von Rechenberg, S. Miettinen, In vivo Effects of Bioactive Glass S53P4 or Beta Tricalcium Phosphate on Osteogenic Differentiation of Human Adipose Stem Cells after Incubation with BMP-2, *J. Stem Cell Res. Ther.* 2 (2012) art. 1000125.
<https://doi.org/10.4172/2157-7633.1000125>
- [64] M.M. Beloti, A.L. Rosa, M. Márcio, A. Beloti, R. Luiz, Osteoblast differentiation of human bone marrow cells under continuous and discontinuous treatment with dexamethasone, *Braz. Dent. J.* 16 (2005) 156-161.
<https://doi.org/10.1590/S0103-64402005000200013>
- [65] Y.P. Chen, Y.L. Chu, Y.H. Tsuang, Y. Wu, C.Y. Kuo, Y.J. Kuo, Anti-Inflammatory Effects of Adenine Enhance Osteogenesis in the Osteoblast-Like MG-63 Cells, *Life* 2020, Vol. 10, Page 116. 10 (2020) 116.
<https://doi.org/10.3390/life10070116>
- [66] A. Suzuki, J. Guicheux, G. Palmer, Y. Miura, Y. Oiso, J.P.P. Bonjour, J. Caverzasio, Evidence for a role of p38 MAP kinase in expression of alkaline phosphatase during osteoblastic cell differentiation, *Bone.* 30 (2002) 91-98.
[https://doi.org/10.1016/S8756-3282\(01\)00660-3](https://doi.org/10.1016/S8756-3282(01)00660-3)
- [67] S. Prabakaran, M. Rajan, C. Lv, G. Meng, Lanthanides-substituted Hydroxyapatite/Aloe vera composite coated titanium plate for bone tissue regeneration, *Int. J. Nanomedicine.* 15 (2020) 8261-8279.
<https://doi.org/10.2147/IJN.S267632>
- [68] M. Ojansivu, A. Mishra, S. Vanhatupa, M. Juntunen, A. Larionova, J. Massera, S. Miettinen, The effect of S53P4-based borosilicate glasses and glass dissolution products on the osteogenic commitment of human adipose stem cells, *PLoS One.* 13 (2018) e0202740.
<https://doi.org/10.1371/journal.pone.0202740>
- [69] P.K. Vallittu, T.O. Närhi, L. Hupa, Fiber glass-bioactive glass composite for bone replacing and bone anchoring implants, *Dent. Mater.* 31 (2015) 371-381.
<https://doi.org/10.1016/j.dental.2015.01.003>

Received on 24-04-2023

Accepted on 26-05-2023

Published on 06-06-2023

DOI: <https://doi.org/10.31875/2410-4701.2023.10.06>© 2023 Alves *et al.*; Zeal Press.

This is an open access article licensed under the terms of the Creative Commons Attribution License (<http://creativecommons.org/licenses/by/4.0/>) which permits unrestricted use, distribution and reproduction in any medium, provided the work is properly cited.